

Article

A Li-Ion Battery State of Charge Estimation Strategy Based on the Suboptimal Multiple Fading Factor Extended Kalman Filter Algorithm

Weibin Wu¹, Jinbin Zeng¹, Qifei Jian², Luxin Tang², Junwei Hou³, Chongyang Han¹, Qian Song¹ and Yuanqiang Luo^{1,*}

¹ College of Engineering, South China Agricultural University, Guangzhou 510642, China; wuweibin@scau.edu.cn (W.W.); jinbinzeng@stu.scau.edu.cn (J.Z.); scauhancy@stu.scau.edu.cn (C.H.); xjc00@stu.scau.edu.cn (Q.S.)

² College of Intelligent Manufacturing and Electrical Engineering, Guangzhou Institute of Science and Technology, Guangzhou 526100, China; tcjqf@scut.edu.cn (Q.J.); tang-luxin@126.com (L.T.)

³ College of Automobile and Engineering Machinery, Guangdong Communication Polytechnic, Guangzhou 510650, China; junweiyou@foxmail.com

* Correspondence: luoyq@scau.edu.cn

Abstract: The state of charge (SOC) is an important indicator for evaluating a battery management system (BMS), which is crucial for the reliability, performance, and life management of a battery. In this paper, the characteristics of a Li-ion battery are deeply studied to explore the charge/discharge curve under different environments. Meanwhile, a second-order RC equivalent circuit model is constructed. The function identification of the EMF and SOC is performed based on the least squares method. The model estimation error is verified by simulation to be less than 0.05 V. Based on the Suboptimal Multiple Fading Factor Extended Kalman Filter (SMFEKF) algorithm, the SOC under constant current and UDDS conditions are estimated. Matlab/simulink simulations illustrate that the estimated accuracy of the proposed algorithm is improved by 79.36% compared with the EKF algorithm. Finally, the validity of the algorithm is verified jointly with the BMS. The results show that the estimation error is within 4% in both constant current condition as well as UDDS conditions, and it can still be predicted quickly and accurately under the uncertainty in the initial value of the SOC.

Keywords: state of charge; charge/discharge curve; SMFEKF; battery management system



Citation: Wu, W.; Zeng, J.; Jian, Q.; Tang, L.; Hou, J.; Han, C.; Song, Q.; Luo, Y. A Li-Ion Battery State of Charge Estimation Strategy Based on the Suboptimal Multiple Fading Factor Extended Kalman Filter Algorithm. *Processes* **2024**, *12*, 998. <https://doi.org/10.3390/pr12050998>

Academic Editor: Hsin-Jang Shieh

Received: 15 April 2024

Revised: 7 May 2024

Accepted: 11 May 2024

Published: 14 May 2024



Copyright: © 2024 by the authors. Licensee MDPI, Basel, Switzerland. This article is an open access article distributed under the terms and conditions of the Creative Commons Attribution (CC BY) license (<https://creativecommons.org/licenses/by/4.0/>).

1. Introduction

With the development of battery management systems (BMSs), the reliability of batteries has been put forward with higher requirements. The functions of BMSs mainly include the data acquisition function, battery state of charge (SOC) estimation, battery state of health (SOH) estimation, safety management, thermal management, energy management, etc. [1]. Among them, battery SOC estimation, as one of the most critical technologies, is the standard for evaluating the remaining power of a power battery and the basis for judging the service life of the battery [2–5].

Currently, the value of the SOC is mostly defined in terms of the remaining battery charge, i.e., the value of the SOC is the percentage of the remaining battery charge to its rated charge under a specific discharge multiplication condition [6], and its expression can be described as:

$$\text{SOC} = \frac{Q_c}{Q_1} \quad (1)$$

where Q_c is the residual current of the battery and Q_1 is the rated capacity of the battery.

The current SOC estimation methods mainly include the ampere–time integration method, the open-circuit voltage (OCV) method, neural networks (NFs), and the Kalman

filtering method. OCV is the most commonly used method for SOC estimation; it has high estimation accuracy but is unable to determine the initial value of the SOC, which leads to a gradual increase in the cumulative error of SOC estimation. The OCV method has the advantage of simplicity but has poor dynamic estimation accuracy and utility. The neural network method requires larger training data and is internally more complex. Kalman filtering is computationally fast, highly accurate, and can improve an algorithm according to different systems [7].

Kalman filtering is widely used in battery SOC estimation, which is characterized by closed-loop control and real-time performance. However, since the Kalman filter cannot be applied to nonlinear systems, more and more scholars have started to study improved Kalman filter algorithms. Wei et al. applied the untraceable Kalman filter algorithm (UKF) to estimate the battery SOC, and the estimation error was about 2%. Y. Leng proposed the capacitive Kalman filter (CKF) for lithium battery SOC estimation, and compared with the untraceable Kalman filter, the estimation error of the volumetric CKF did not exceed 2% at most, and the accuracy was 1% higher. L. Leng proposed the volumetric CKF for lithium battery SOC estimation. The estimation error of volumetric Kalman filtering did not exceed 2% at most, and the accuracy was 1% higher. L. Ji proposed the adaptive extended Kalman filtering (AEKF) algorithm, which estimated the mean and variance of unknown noise in real time and improved estimation accuracy compared with traditional extended Kalman filtering. Y.X. Xiong estimated the SOC of Li-ion batteries based on the dual Kalman filtering algorithm, and the estimated absolute error was less than 0.01%, while the estimated error was more than 0.01% and the absolute error was less than 0.019, which had high accuracy. Rui Xiong designed the Robust Extended Kalman Filter (REKF) method based on the DP model to estimate the SOC and determined the accuracy of the estimation by performing Federal Urban Driving Schedule (FUDS) experiments. In addition to the above algorithms, there are other improved Kalman filtering algorithms aimed at improving SOC estimation accuracy [8–16].

This paper is organized as follows. In Section 2, battery capacity influencing factors are analyzed, and the correction coefficients of discharge point multiplication and temperature on capacity are calculated to derive the SOC revised form under different influencing factors. In Section 3, the battery model and parameter identification are established, the second-order RC network equivalent circuit battery model is established, the functional relationship between the EMF and SOC is obtained based on the least squares method through experimental data of open-circuit voltage measurement, and the accuracy of the model is verified through a pulse discharge experiment. In Section 4, the SMFEKF algorithm is designed based on the second-order RC equivalent circuit model, and the accuracy and feasibility of the SMFEKF algorithm are simulated and verified in Matlab/simulink. In Section 5, the SOC estimation algorithm is further validated by building a BMS platform.

2. Battery Characterization

2.1. Charge/Discharge Experimental Platform

The experimental platform consists of a battery test system, a high- and low-temperature test chamber, an upper computer, and a lithium ternary battery. Among them, the BMS is connected to the upper computer through a CAN bus. The high- and low-temperature test chamber controls the temperature of the test environment. For the selected lithium ternary battery, the main parameters are shown in Table 1. Its cathode is $\text{Li}(\text{NiCoMn})\text{O}_2$, a lithium nickel manganese cobalt oxide (NMC) battery. NMC is a Li-ion battery with a different type of cathode. Unlike lithium iron phosphate (LFP), which possesses good capacity and stability, NMC demonstrates an improved cycle life, thermal stability, and energy density [17]. The battery test system (BTS) is a BNT series of power battery test equipment, produced by the German Decathlon Group, with working condition simulation and battery charge/discharge test functions; the specific parameters are shown in Table 1. The software used in the upper computer is the BTS-600 (https://www.digatron.com/Portals/38/Images/documents/PRODUKTBLATT_UBT_EN.PDF?ver=2019-06-12-091045-427) bat-

tery testing system; by programming the test software, the battery testing system can be made to run the test according to the program under different control conditions. The constant temperature and humidity test chamber can control the humidity of the room and the current temperature of the experimental environment so that the battery is charged and discharged at a constant temperature.

Table 1. Parameters of the tested battery.

	Item	Parameter
Lithium-ion battery (NMC)	Electrode materials	Li(NiCoMn)O ₂
	Rated capacity	11 Ah
	Standard discharge current	0.2 C~1 C
	Discharge temperature	−10 °C~60 °C
	Discharge cut-off voltage	3.0 V
	Standard voltage	3.7 V
	Standard charge current	0.2 C~1 C
	Cycle life (1 C/1 C, 100% DOD)	2000 cycles
	Charge cut-off voltage	4.2 V
BTS	Used voltage range	0–100 V
	Charge and discharge current range	1–200 A
	Accuracy of current and voltage	1% (full-scale)
	Sample time	20 ms
	Temperature	10–40 °C

2.2. Discharge Experiments at Various Discharge Rates

Under the external temperature of 25 °C, the discharge test of the ternary lithium battery with different discharge multiplicity is conducted, and the curves of battery capacity and discharge multiplicity are obtained, as shown in Figure 1a. The results show that with all other things being equal, the larger the discharge multiplier, the smaller the amount of power discharged by the battery. The ternary lithium-ion battery is discharged at different temperatures (10 °C, 25 °C, 40 °C) at a constant current with a 1 C discharge multiplier to obtain the terminal voltage versus time curves of the battery at different temperatures, as shown in Figure 1b.

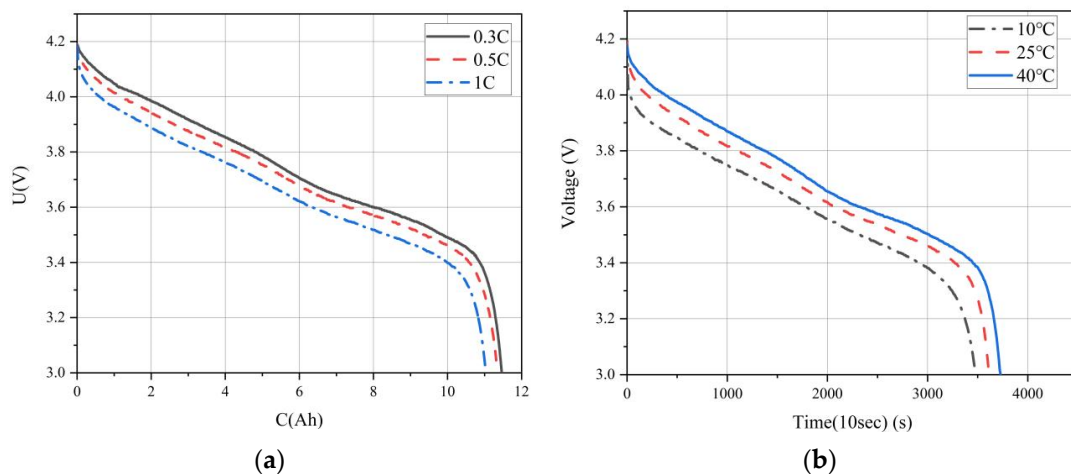


Figure 1. Li-ion battery capacity influence factor analysis curve. (a) C-U curves with different multiplication rates. (b) T-U curves at different temperatures.

It is assumed that the discharge multiplier is 1 C, the temperature is 25 °C, and the capacity correction factor $K_1 = 1$, where the capacity correction factor K_i means the ratio of the capacity of the battery when the discharge multiplication rate is “i” to the capacity of the battery when “i = 1”. The calculation results of the capacity correction coefficient when

the discharge multiplication rate is 0.3 C, 0.5 C, and 1 C are shown in Table 2. Second-order fitting is carried out, which results in the curve of the capacity correction coefficient K_i , as shown in Figure 2. The expression is:

$$K_i[i(t)] = -0.0001[i(t)]^2 - 0.0035i(t) + 1.053 \quad (2)$$

Table 2. Discharge rate and the battery capacity correction factor.

Discharge rate (Ah)	3	5.5	11
Capacity correction factor (K_i)	1.04	1.03	1

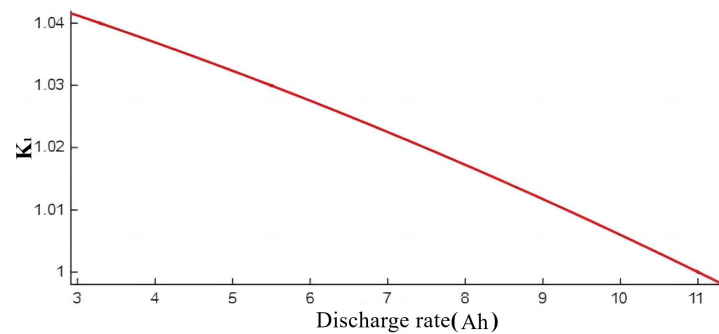


Figure 2. Discharge multiplier and capacity correction factor relationship curve.

2.3. Temperature Discharge Experiments at Different Temperatures

The internal chemical reaction of the battery at different temperatures is very different, and the actual working performance is also different. Discharge test experiments are carried out on the battery at different temperatures. The test results are shown in Figure 1b, from which it can be seen that under the condition of the same discharge multiplier, the higher temperature, the greater the amount of power discharged by the battery.

Using 25 °C as the discharge capacity benchmark, the accuracy of SOC estimation at different temperatures was improved by using the temperature correction factor K_T , which represents the ratio of the battery discharge capacity to the benchmark value at different temperatures. The statistics of the fitting results are shown in Table 3. The fitting results are shown in Figure 3. The fitting polynomial is:

$$K_T[T(t)] = -0.00004[T(t)]^2 - 0.0048T(t) + 0.9056 \quad (3)$$

Table 3. Temperature and the temperature correction factor.

Temperature ($T/^\circ\text{C}$)	10	25	40
Temperature correction factor (K_T)	0.95	1	1.03

According to the ampere–time integration method, the equation of state of the battery SOC is:

$$\text{SOC}(t) = \text{SOC}_0 - \frac{\int_{t_0}^t \eta \times I(t) dt}{C_N} \quad (4)$$

where C_N represents the battery calibration capacity, $I(t)$ represent the operating current of the battery, and η represents the charging and discharging efficiency.

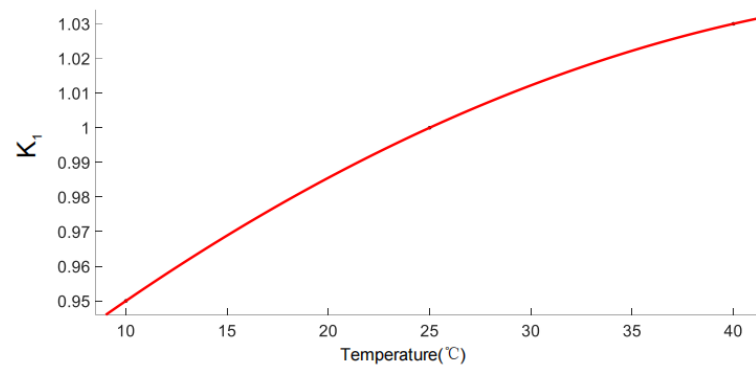


Figure 3. Temperature correction coefficient relationship curve.

The aging as well as self-discharge phenomena of the battery are internal properties of the battery that cannot be avoided and are not analyzed in this paper. After considering the effects of temperature and charge/discharge multiplication on the battery capacity [18], the calculation equation of SOC is corrected as:

$$SOC(t) = SOC_0 - \frac{K_1 K_T \int_{t_0}^t \eta \times I(t) dt}{C_N} \quad (5)$$

3. Establishment of the Battery Model and Parameter Identification

3.1. Equivalent Circuit Modeling

In order to research the external characteristics of the battery and make the electrochemical model expression easy to calculate, in this paper, the second-order RC equivalent circuit model is improved by connecting a resistive–capacitive loop in series with the Thevenin model [19,20], as shown in Figure 4. Since the capacitor has infinite resistance, the voltage applied to the capacitor is the electric potential, which is described by $EMF = f(SOC)$ [21].

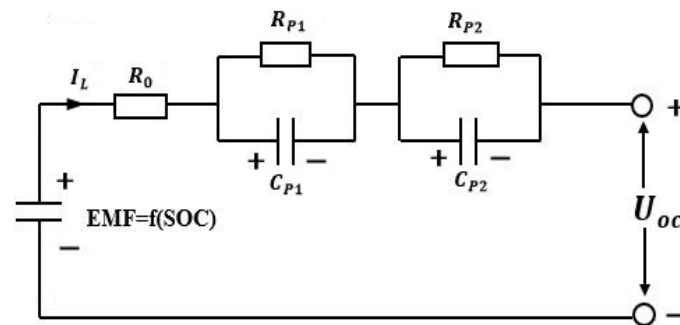


Figure 4. Lithium-ion power battery model structure.

In Figure 4, EMF denotes the electric potential of the battery as a function of the SOC of the battery, which is expressed by $EMF = f(SOC)$.

The equations for the above equivalent circuit model can be derived from Kirchhoff's law as:

$$\begin{aligned} U_{OC} &= EMF - R_0 I_L - U_{P1} - U_{P2} \\ U'_{P1} &= -\frac{U_{P1}}{R_{P1} C_{P1}} + \frac{I_L}{C_{P1}} \\ U'_{P2} &= -\frac{U_{P2}}{R_{P2} C_{P2}} + \frac{I_L}{C_{P2}} \end{aligned} \quad (6)$$

where R_0 denotes the ohmic internal resistance of the battery, which is used to describe the resistance generated during the chemical reactions and ionic motion inside the battery. The two resistive–capacitive networks (RC networks) mentioned above are used to describe the polarized internal resistance of the battery, in which R_{P1} and C_{P1} denote the electrochemical

polarization of the battery; R_{P2} and C_{P2} denote the concentrated polarization of the battery; U_{OC} denotes the open-circuit voltage of the battery; U_{P1} and U_{P2} denote the voltage across the polarization capacitor; U'_{P1} and U'_{P2} denote the derivatives of U_{P1} and U_{P2} with respect to time, respectively; and I_L denotes the load current in the circuit.

3.2. Parameter Identification

The traditional algorithm for the parameter identification process has the problem of low accuracy, which leads to the accumulation of errors. In this paper, the least squares method is used to identify the battery model parameters. From 10% to 90%, nine SOC points are selected for experimental testing, and the least squares method is used to fit the parameters to $EMF = f(SOC)$. The fitting error is:

$$\delta_i = \phi(x_i) - f(x_i) (i = 1, \dots, m) \quad (7)$$

The curve fitted by the principle of least squares should satisfy:

$$S(a_0, a_1, \dots, a_n) = \sum_{i=1}^m [a_0\phi_0(x_i) + a_1\phi_1(x_i) + \dots + a_n\phi_n(x_i) - y_i]^2 = \min \quad (8)$$

where δ is the error of the fitted curve; $\phi(x_i)$ is the value of the fitted function at x_i ; $f(x_i)$ denotes the value of the discrete function at x_i ; and S is a collection of the factors to determine " a_0, a_1, \dots, a_n ".

A ternary lithium battery is selected, with a rated capacity of 11 Ah and an operating voltage range of 3.0 V–4.2 V. The relationship between the OCV and SOC during the charging and discharging of the battery is tested separately, and the test results are shown in Table 4. The values of EMF corresponding to different SOC values are obtained, as shown in Table 5.

Table 4. OCV and SOC values.

SOC	Discharge/V	Charge/V	Average/V
0.9	4.059	4.056	4.058
0.8	4.003	3.997	4.000
0.7	3.925	3.921	3.923
0.6	3.862	3.856	3.859
0.5	3.761	3.751	3.756
0.4	3.679	3.682	3.681
0.3	3.636	3.640	3.638
0.2	3.594	3.603	3.599
0.1	3.528	3.525	3.527

Table 5. EMF and SOC values.

Variable	Sampling Point								
SOC	0.9	0.8	0.7	0.6	0.5	0.4	0.3	0.2	0.1
EMF	4.058	4.000	3.923	3.859	3.756	3.681	3.638	3.599	3.527

The experimental data from the above table are applied to fit the parameters to the coefficients to be determined in the expression. The polyfit function is used to derive the expression $EMF = f(SOC)$ as follows:

$$EMF = -0.572391SOC^3 + 1.05177SOC^2 + 0.124234SOC + 3.51594 \quad (9)$$

$$EMF = 14.5833SOC^5 - 39.6402SOC^4 + 39.2519SOC^3 - 16.9309SOC^2 + 3.61746SOC + 3.29892 \quad (10)$$

$$\text{EMF} = -0.374\text{SOC}^7 + 1.3015\text{SOC}^6 - 1.8258\text{SOC}^5 + 1.3186\text{SOC}^4 - 0.5193\text{SOC}^3 + 0.1092\text{SOC}^2 - 0.0106\text{SOC} + 0.0039 \quad (11)$$

According to the fitting results in Table 6, it can be seen that the higher the polynomial order, the higher the fitting accuracy, but this result is easily oscillated. The closer the R-square value is to ± 1 , the better the curve fit. The comprehensive analysis of this paper uses the fifth-order polynomial to fit the expression of $\text{EMF} = f(\text{SOC})$, where SSE denotes the sum of squares due to error, RMSE denotes root mean squared error, and R-square denotes the coefficient of determination.

Table 6. Error values for each order of fit.

Fitting Order	SSE	RMSE	R-Square
Third-order fitting	0.001259	0.011828	0.99550
Fourth-order fitting	0.000221	0.004956	0.99921
Fifth-order fitting	0.000052	0.002406	0.99981

3.3. Identification of Other Parameters

The HPPC is performed on the battery. The pulse discharge curve at $\text{SOC} = 0.8$ is used in conjunction with the least squares method to identify the parameters of the ohmic internal resistance (R_0), the two polarization internal resistances (R_{P1} , R_{P2}), and the polarization capacitance (C_{P1} , C_{P2}) in the second-order RC model. The results are shown in Table 7.

Table 7. Second-order RC equivalent circuit model parameter identification results.

SOC	$R_0/\text{m}\Omega$	$R_{P1}/\text{m}\Omega$	C_{P1}/F	$R_{P2}/\text{m}\Omega$	C_{P2}/F
0.9	4.13	0.33	1151.52	4.00	3492.5
0.8	4.01	0.22	2182.82	3.9	3400.00
0.7	4.13	0.21	1952.38	3.5	3054.29
0.6	4.09	0.48	833.33	3.5	3231.42
0.5	4.32	0.45	555.56	3.7	3583.78
0.4	4.18	0.28	1392.86	2.9	3968.97
0.3	3.86	0.33	1212.12	3.2	4371.88
0.2	4.63	0.31	1193.55	3.3	4884.85

3.4. Accuracy Verification

In order to verify the accuracy of the least squares parameter identification results used in this paper, a simulation model is built in Matlab, and the battery model is verified under HPPC pulse discharge. The experimental results are shown in Figure 5a.

The pulse discharge curve at $\text{SOC} = 0.8$ is selected, as shown in Figure 5b. During the pulse discharge, the error is at 0.03 V–0.04 V, and the polarization phenomenon of the battery is ignored during the experimental measurement because of the presence of the polarization internal resistance. By the later zero-state response interval, the error is close to 0.01 V, and the overall error remains within 0.05 V. As verified above, the model is valid.

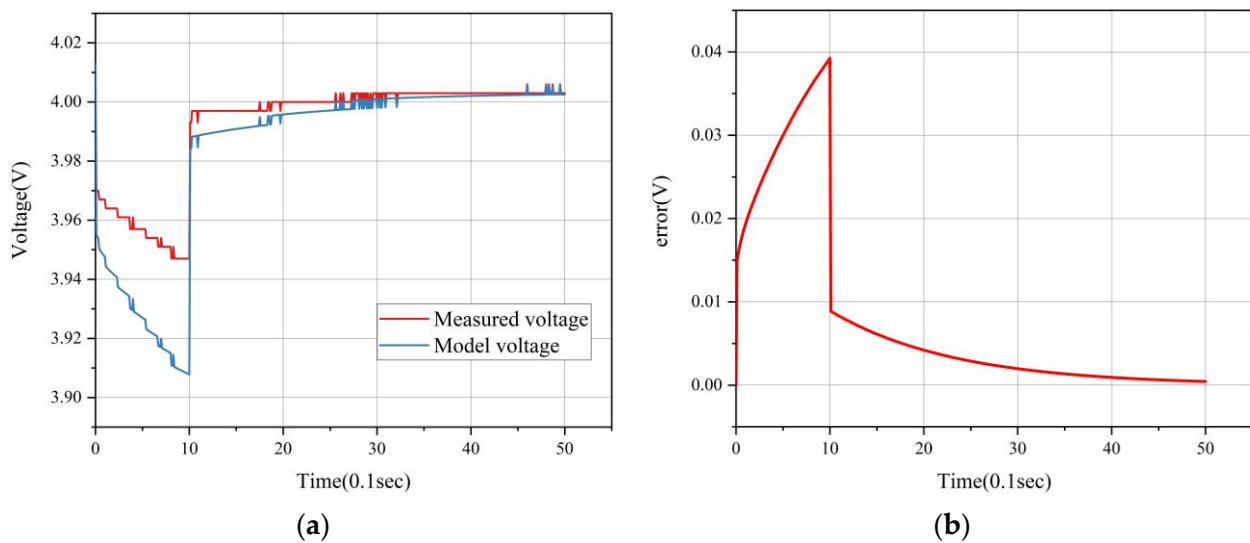


Figure 5. HPPC pulse discharge test. (a) Pulse discharge voltage curve. (b) Pulse discharge error.

4. SOC Estimation Based on the SMFEKF Algorithm

Classical Kalman filtering is mostly used for the state estimation of linear systems; however, the SOC of a battery often behaves as a nonlinear system under the operating condition. EKF is used to filter a nonlinear system into an approximately linear system, and then the state estimation is completed by using classical Kalman filtering. However, when Taylor series expansion is performed for the first-order linearization truncation, the large estimation error of the higher-order terms is neglected, which is likely to lead to problems such as filter divergence.

Therefore, this paper proposes a Suboptimal Multiple Fading Factor Extended Kalman Filter (SMFEKF) algorithm [22]. By introducing multiple fading factors into the state prediction error covariance array, the fading factors are able to fade out different state data at different rates to improve the tracking capability of the system. The error covariance equation of the algorithm after the introduction of the fading factors is:

$$P_{k|k-1} = \lambda_k A_{k|k-1} P_{k-1|k-1} A_{k|k-1}^T + T_{k|k-1} Q_{k-1} T_{k|k-1}^T \quad (12)$$

where $\lambda_k = \text{diag}[\lambda_k^1, \lambda_k^2, \dots, \lambda_k^n]$ is the suboptimal multiple fading factor diagonal matrix, $\lambda_k^i \geq 1 (i = 1, 2, \dots, n)$, corresponding to n state channels.

By using U_{P1} and U_{P2} in the second-order RC equivalent circuit model as the state variables of the system, the input quantity as the charging and discharging currents, and the open-circuit voltage, U_{OC} , as the output quantity, the discretized state equations and observation equations can be derived as:

$$\begin{cases} SOC(k) = SOC(k-1) - \frac{k_I k_T \Delta t}{C_N} I_L(k-1) \\ U_{P1}(k) = U_{P1}(k-1) e^{-\frac{\Delta t}{\tau_1}} + R_{P1} (1 - e^{-\frac{\Delta t}{\tau_1}}) I_L(k-1) \\ U_{P2}(k) = U_{P2}(k-1) e^{-\frac{\Delta t}{\tau_2}} + R_{P2} (1 - e^{-\frac{\Delta t}{\tau_2}}) I_L(k-1) \end{cases} \quad (13)$$

$$U_{OC}(k) = EMF(SOC(k)) - R_O I_L(k) - U_{P1}(k) - U_{P2}(k) + v_k \quad (14)$$

where Δt is the time interval of the sampling sequence, τ is the time response constant, and $\tau_1 = R_{P1} C_{P1}$.

Taking the discretized state equations into the nonlinear system, the state variables of the corresponding system is:

$$x_k = [SOC(k), U_{P1}(k), U_{P2}(k)]^T \quad (15)$$

where the input is $u_k = I_L(k)$, the corresponding nonlinear function is:

$$f(x_k, u_k) = \begin{bmatrix} 1 & 0 & 0 \\ 0 & e^{-\frac{\Delta t}{\tau_1}} & 0 \\ 0 & 0 & e^{-\frac{\Delta t}{\tau_2}} \end{bmatrix} \times \begin{bmatrix} \text{SOC}(k-1) \\ U_{P1}(k-1) \\ U_{P2}(k-1) \end{bmatrix} + \begin{bmatrix} -\frac{k_I k_T \Delta t}{C_N} \\ R_{P1}(1 - e^{-\frac{\Delta t}{\tau_1}}) \\ R_{P2}(1 - e^{-\frac{\Delta t}{\tau_2}}) \end{bmatrix} I_L(k-1) \quad (16)$$

$$h(x_k, u_k) = \text{EMF}(\text{SOC}(k)) - R_O I_L(k) - U_{P1}(k) - U_{P2}(k) \quad (17)$$

where the corresponding matrices A_k , B_k , H_k , and D_k are:

$$A_k = \left. \frac{\partial f(x_k, u_k)}{\partial x_k} \right|_{x_k = \hat{x}_k} = \begin{bmatrix} 1 & 0 & 0 \\ 0 & e^{-\frac{\Delta t}{\tau_1}} & 0 \\ 0 & 0 & e^{-\frac{\Delta t}{\tau_2}} \end{bmatrix}; \quad B_k = \begin{bmatrix} -\frac{k_I k_T \Delta t}{C_N} \\ R_{P1}(1 - e^{-\frac{\Delta t}{\tau_1}}) \\ R_{P2}(1 - e^{-\frac{\Delta t}{\tau_2}}) \end{bmatrix} \quad (18)$$

$$H_k = \left. \frac{\partial h(x_k, u_k)}{\partial x_k} \right|_{x_k = \hat{x}_k} = \begin{bmatrix} \frac{\partial \text{EMF}}{\partial \text{SOC}} & -1 & -1 \end{bmatrix}; \quad D_k = -R_O \quad (19)$$

The computational procedure of the specific SMFEKF algorithm is as follows:

Step 1: Initialization. Assign initial values to the system's state variable x_0 , error covariance P_0 , system disturbance covariance array Q_0 , and observation noise covariance array R_0 .

Step 2: System state vector update.

$$\begin{cases} \hat{x}_{k|k-1} = f(\hat{x}_{k-1|k-1}, u_{k-1}) + w_k \\ P_{k|k-1} = \lambda_k A_{k|k-1} P_{k-1|k-1} A_{k|k-1}^T + T_{k|k-1} Q_{k-1} T_{k|k-1}^T \\ K_k = P_{k|k-1} H_k^T (H_k P_{k|k-1} H_k^T + R_k)^{-1} \\ \hat{x}_{k|k} = \hat{x}_{k|k-1} + H_k Y_k \\ Y_k = Z_k - H(\hat{x}_{k|k-1}, u_k) \\ P_{k|k} = (E - K_k H_k) P_{k|k-1} \end{cases} \quad (20)$$

5. Testing and Analysis

5.1. SOC Estimation by SMFEKF

In order to verify the effectiveness of the algorithms, the EKF and SMFEKF algorithms are used for simulation comparison. The initial value of the SOC is set to 1, the circuit is in the open circuit state, the terminal voltage of the RC link is 0, the initial value of the state variable is $[1 \ 0 \ 0]^T$, and the initial mean squared error is $P_0 = 10^{-6} \times [1 \ 0 \ 0; 0 \ 1 \ 0; 0 \ 0 \ 1]$. The error covariance of process noise and the error covariance of measurement noise are taken according to empirical parameters. $Q_k = 10^{-6}$, $R_k = 0.05$.

The simulation verification is carried out at 25 °C and 0.5 C constant current discharge conditions, and the simulation results of the two algorithms are shown in Figure 6. From the curves in Figure 6a, it can be seen that the EKF algorithm has a strong tracking ability to the actual SOC at 1000 s and gradually deviates from the reference value later on, with the largest error between 3000 s and 4000 s. The SMFEKF algorithm estimation results are extremely close to the reference value, and the algorithm has strong tracking. From Figure 6b, it can be seen that the absolute error of SOC estimation based on the SMFEKF algorithm is closer to the zero value than that of the EKF algorithm, indicating that the SOC estimation is closer to the real value and converges faster.

In order to demonstrate more intuitively the improvement in the SOC estimation accuracy by this paper's algorithm, the maximum absolute error \root mean square error and mean error of the SMFEKF algorithm and EKF are compared, and the results are shown in Table 8.

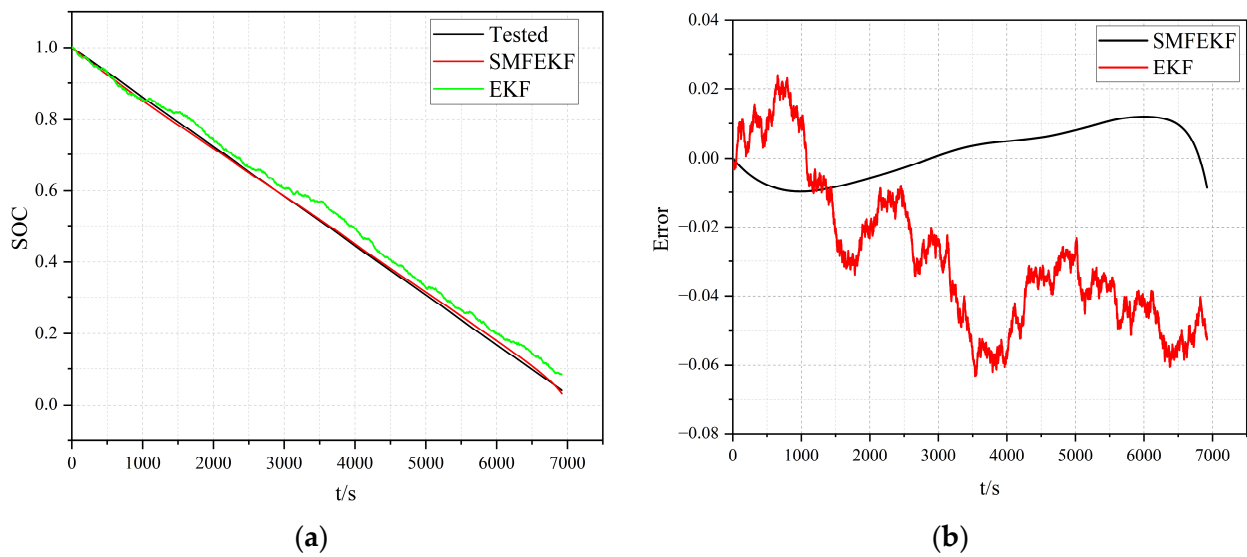


Figure 6. Simulation comparison of the EKF and SMFEKF algorithms under 0.5 C constant current discharge conditions. (a) Comparison of SOC estimates. (b) Estimation error.

Table 8. Comparison of estimation errors of the EKF and SMFEKF algorithms.

	ϵ_{\max}	RMSE	MAE
EKF	0.06327	0.03571	0.031692
SMFEKF	0.11873	0.00737	0.001295

As shown in Table 8, the maximum error ϵ_{\max} , the root means square error RMSE, and the mean error MAE estimated by the SMFEKF algorithm are smaller than that of the EKF algorithm. The RMSE of the SOC estimation of the SMFEKF algorithm is 0.00737, which is an improvement in the estimation accuracy by 79.36% compared with the 0.03571 of the EKF algorithm. From the above analysis, it can be seen that the SMFEKF algorithm has better stability performance and higher accuracy.

5.2. Algorithm Validation in Conjunction with BMS Platforms

In order to verify the feasibility and accuracy of the battery SOC estimation algorithm, a BMS platform was constructed, including a battery pack formed by a series connection of four 11 Ah Li-ion batteries, a main control board, an acquisition board, a CAN line, and a host computer. Experiments were conducted on the battery pack at constant current discharge and UDDS using a current of 1 C, and then the test results were compared and analyzed with the real value of the SOC of the battery pack. The test results are shown in Figures 7 and 8.

The experimental results show that the maximum error of the algorithm estimation is within 4% under the constant current discharge condition, which is in line with the international standard within 5%. The initial value of the algorithm deviates 45% from the experimental initial value under the UDDS condition, but the initial value converges very quickly in a short period of time, which demonstrates that the algorithm proposed in this paper is still effective when the initial SOC value is unknown or incorrect.

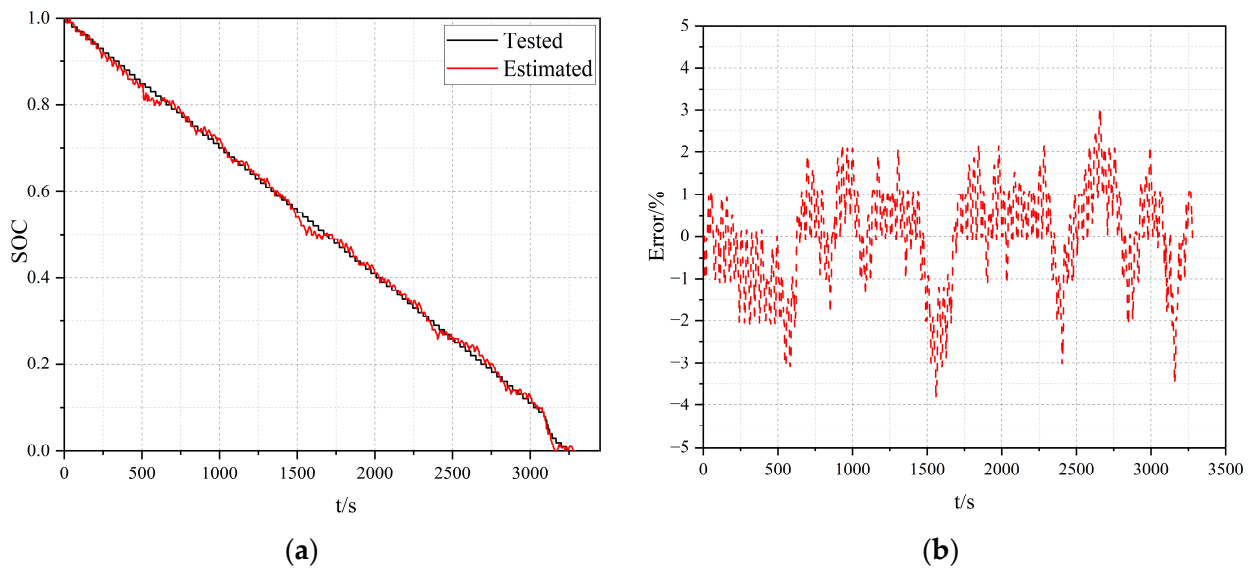


Figure 7. Constant current discharge condition SOC estimation results. (a) Estimated value of the SOC. (b) Estimation error.

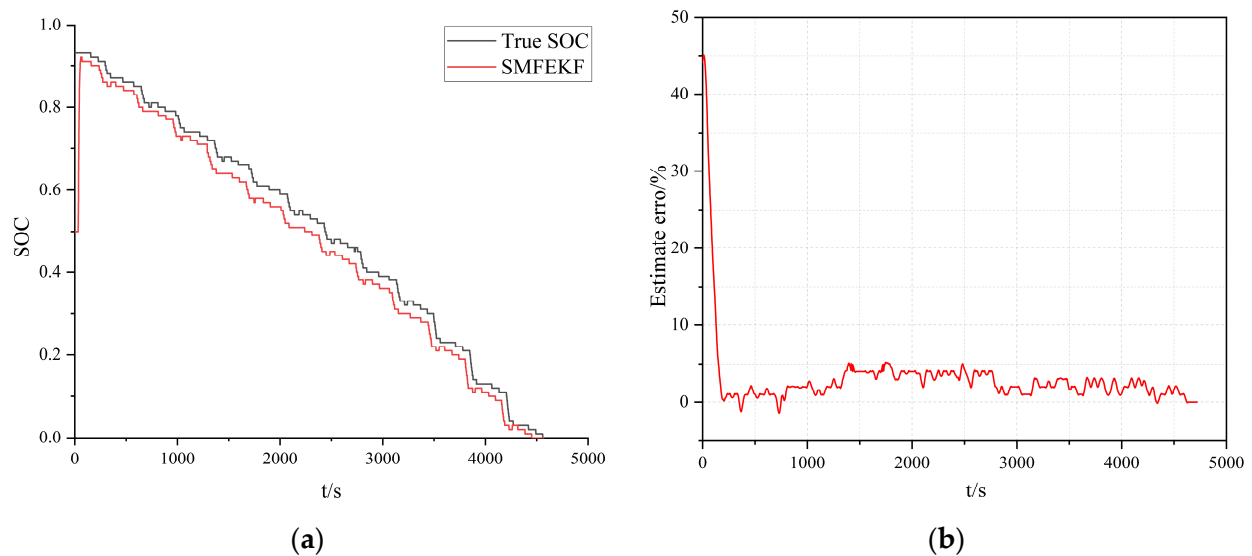


Figure 8. UDDS operating conditions and SOC estimation results. (a) Estimated value of the SOC. (b) Estimation error.

6. Conclusions

Aiming to address the problems of existing SOC estimation methods, such as the accumulation of errors resulting from non-determinable model parameters, this paper proposes a SOC estimation method based on the SMFEKF algorithm and the least squares method. Firstly, the different factors affecting the battery capacity are analyzed by building a battery charging and discharging test platform. The correction coefficients of multiplicity and temperature on the battery capacity are derived through experiments, and the SOC calculation equation is corrected. The second-order RC network equivalent circuit model is selected as the estimation model of the SOC, combined with the least squares method to identify the model parameters, and the pulse discharge simulation test is carried out by Matlab. The test results show that at the beginning of pulse discharge, the error is in the range of 0.03 V~0.04 V, the error is close to 0.01 V in the back of the zero state response interval, and the overall error is kept within 0.05 V, which has high accuracy. The overall error remains within 0.05 V, with high accuracy.

In order to verify the estimation effect of the algorithms, the EKF and SMFEKF algorithms are simulated and analyzed in Matlab. The experimental results show that the estimation error of the SMFEKF algorithm under the constant current discharge condition improves the estimation accuracy by 79.36% compared with the EKF algorithm. Finally, the algorithm is further verified in combination with the EMS platform, indicating that the algorithm is still able to make fast and accurate predictions under the uncertainty in the initial value of the SOC. Therefore, it can be said that the algorithm proposed in this paper is an estimation method with high accuracy and good robustness.

Author Contributions: The presented work was completed under the supervision of Y.L. and W.W. The other author contributions include the following: Y.L. and W.W.: conceptualization, methodology, software, and writing—review; J.Z.: conceptualization, methodology, software, and writing—original draft; Q.J. and L.T.: validation, writing—review and editing; C.H. and Q.S.: methodology and writing—review; J.H.: project management and financial support. All authors have read and agreed to the published version of the manuscript.

Funding: This research was funded by Key Technologies R&D Program of Guangdong Province: 2021B0101220003; Key Technologies R&D Program of Guangdong Province: 2020B090926004; Department of Education of Guangdong Province Project: 2021KQNCX008; and the Department of Education of Guangdong Province Project: 2023KQNCX187.

Data Availability Statement: The data that support the findings of this study are available on request from the author, [J.Z.], upon reasonable request.

Acknowledgments: The authors acknowledge the editors and reviewers for their constructive comments and support of this work.

Conflicts of Interest: The authors declare no conflicts of interest.

Abbreviations

AEKF	adaptive extended Kalman filtering
BMS	battery management system
BTS	battery test system
CKF	capacitive Kalman filter
EKF	extended Kalman filtering
EMF	electromotive force
NF	neural network
OCV	open-circuit voltage
SMFEKF	Suboptimal Multiple Fading Factor Extended Kalman Filter
SOC	state of charge
SOH	battery state of health
UDDS	Urban Dynamometer Driving Schedule

References

- Lu, L.; Han, X.; Li, J.; Hua, J.; Ouyang, M. A review on the key issues for lithium-ion battery management in electric vehicles. *J. Power Sources* **2013**, *226*, 272–288. [[CrossRef](#)]
- Zou, Y.; Hu, X.; Ma, H.; Li, S. Combined State of Charge and State of Health estimation over lithium-ion battery cell cycle lifespan for electric vehicles. *J. Power Sources* **2015**, *273*, 793–803. [[CrossRef](#)]
- Meng, J.; Ricco, M.; Luo, G.; Swierczynski, M.; Stroe, D.I.; Stroe, A.I.; Teodorescu, R. An overview and comparison of online implementable SOC estimation methods for lithium-ion battery. *IEEE Trans. Ind. Appl.* **2017**, *54*, 1583–1591. [[CrossRef](#)]
- Zhang, R.; Xia, B.; Li, B.; Cao, L.; Lai, Y.; Zheng, W.; Wang, H.; Wang, W. State of the Art of Lithium-Ion Battery SOC Estimation for Electrical Vehicles. *Energies* **2018**, *11*, 1820. [[CrossRef](#)]
- Jiang, Y.; Wang, C.; Kong, J.; Li, j.; Zhou, F. Advances in SOC estimation methods for lithium-ion batteries. *Chin. J. Power Supply Technol.* **2018**, *42*, 296–300.
- Tong, S.; Klein, M.P.; Park, J.W. On-line optimization of battery open circuit voltage for improved state-of-charge and state-of-health estimation. *J. Power Sources* **2015**, *293*, 416–428. [[CrossRef](#)]
- Yang, W.; Zhu, S.; Chen, Y.; Zhu, J.; Xue, L. Estimation of SOC of lithium-ion battery packs based on improved ampere-time integration method. *Chin. J. Power Supply Technol.* **2018**, *42*, 183–184.

8. Sepasi, S.; Ghorbani, R.; Liaw, B.Y. Improved extended Kalman filter for state of charge estimation of battery pack. *J. Power Sources* **2014**, *255*, 368–376. [[CrossRef](#)]
9. Len, Y. Estimation of Lithium Battery SOC Based on CKF and the Research of Battery Management System. Ph.D. Dissertation, Jiangsu University, Zhenjiang, China, 2016.
10. Ji, L.; Chellali, R. State of charge estimation of battery based on adaptive extended Kalman filter. *Chin. J. Batter.* **2018**, *48*, 240–243.
11. Wei, J.; Fu, Z. Traceless Kalman Filtering for Lithium Battery State of Charge Estimation. *Chin. J. J. Henan Univ. Sci. Technol. (Nat. Sci.)* **2018**, *39*, 45–49.
12. Liu, S.; Yu, Y.; Li, H.; Li, Y.; Zhao, Z. Estimation of state of charge for lithium battery based on unscented Kalman filter. *Chin. J. Power Supply Technol.* **2018**, *42*, 40–45.
13. Gu, Y.; Zhang, Y. Estimation of state of charge of lithium-ion battery based on dual extend Kalman filter. *Chin. J. Power Supply Technol.* **2016**, *40*, 986–989.
14. Wang, L.; Lu, D.; Liu, L.; Liu, Q.; Liu, L.; Zhao, X. State of charge estimation for LiFePO₄ battery via dual extended kalman filter and charging voltage curve. *Electrochim. Acta* **2019**, *296*, 1009–1017. [[CrossRef](#)]
15. Li, S.; Hu, M.; Li, Y.; Gong, C. Fractional-order modeling and SOC estimation of lithium-ion battery considering capacity loss. *Int. J. Energy Res.* **2018**, *43*, 417–429. [[CrossRef](#)]
16. He, H.; Xiong, R.; Fan, J. Evaluation of Lithium-Ion Battery Equivalent Circuit Models for State of Charge Estimation by an Experimental Approach. *Energies* **2011**, *4*, 582–598. [[CrossRef](#)]
17. Tran, M.-K.; DaCosta, A.; Mevawalla, A.; Panchal, S.; Fowler, M. Comparative Study of Equivalent Circuit Models Performance in Four Common Lithium-Ion Batteries: LFP, NMC, LMO, NCA. *Batteries* **2021**, *7*, 51. [[CrossRef](#)]
18. Tian, Y. Multi-Model Adaptive Kalman Filtering SOC Estimation Considering Battery Temperature and Rate Characteristics. Ph.D. Dissertation, Hunan University, Changsha, China, 2018.
19. Fang, Y.; Cheng, X.; Yin, Y. SOC estimation of lithium-ion battery packs based on Thevenin model. *Appl. Mech. Mater.* **2013**, *299*, 211–215. [[CrossRef](#)]
20. Putra, W.S.; Dewangga, B.R.; Cahyadi, A.; Wahyunggoro, O. Current estimation using Thevenin battery model. In Proceedings of the Joint International Conference on Electric Vehicular Technology and Industrial, Mechanical, Electrical and Chemical Engineering (ICEVT & IMECE), Surakarta, Indonesia, 4–5 November 2015; IEEE: Piscataway, NJ, USA, 2015; pp. 5–9.
21. Li, D.; Ouyang, J.; Li, H.; Xie, J. Accuracy state of charge estimation used in energy storage system for electric transportation. In Proceedings of the Conference and Expo Transportation Electrification Asia-Pacific (ITEC Asia-Pacific), Beijing, China, 31 August–3 September 2014; IEEE: Piscataway, NJ, USA, 2014; pp. 1–6.
22. Selvaraj, V.; Vairavasundaram, I. A comprehensive review of state of charge estimation in lithium-ion batteries used in electric vehicles. *J. Energy Storage* **2023**, *72*, 108777. [[CrossRef](#)]

Disclaimer/Publisher’s Note: The statements, opinions and data contained in all publications are solely those of the individual author(s) and contributor(s) and not of MDPI and/or the editor(s). MDPI and/or the editor(s) disclaim responsibility for any injury to people or property resulting from any ideas, methods, instructions or products referred to in the content.